NASA/TM—2005-213359

Estimation of ZnSe Slow-Crack-Growth Properties for Design of the Flow Enclosure Accommodating Novel Investigations in Combustion of Solids (FEANICS) Windows

Jonathan A. Salem
Glenn Research Center, Cleveland, Ohio

April 2005

The NASA STI Program Office . . . in Profile

Since its founding, NASA has been dedicated to the advancement of aeronautics and space science. The NASA Scientific and Technical Information (STI) Program Office plays a key part in helping NASA maintain this important role.

The NASA STI Program Office is operated by Langley Research Center, the Lead Center for NASA's scientific and technical information. The NASA STI Program Office provides access to the NASA STI Database, the largest collection of aeronautical and space science STI in the world. The Program Office is also NASA's institutional mechanism for disseminating the results of its research and development activities. These results are published by NASA in the NASA STI Report Series, which includes the following report types:

- TECHNICAL PUBLICATION. Reports of completed research or a major significant phase of research that present the results of NASA programs and include extensive data or theoretical analysis. Includes compilations of significant scientific and technical data and information deemed to be of continuing reference value. NASA's counterpart of peer-reviewed formal professional papers but has less stringent limitations on manuscript length and extent of graphic presentations.

- TECHNICAL MEMORANDUM. Scientific and technical findings that are preliminary or of specialized interest, e.g., quick release reports, working papers, and bibliographies that contain minimal annotation. Does not contain extensive analysis.

- CONTRACTOR REPORT. Scientific and technical findings by NASA-sponsored contractors and grantees.

- CONFERENCE PUBLICATION. Collected papers from scientific and technical conferences, symposia, seminars, or other meetings sponsored or cosponsored by NASA.

- SPECIAL PUBLICATION. Scientific, technical, or historical information from NASA programs, projects, and missions, often concerned with subjects having substantial public interest.

- TECHNICAL TRANSLATION. English-language translations of foreign scientific and technical material pertinent to NASA's mission.

Specialized services that complement the STI Program Office's diverse offerings include creating custom thesauri, building customized databases, organizing and publishing research results . . . even providing videos.

For more information about the NASA STI Program Office, see the following:

- Access the NASA STI Program Home Page at ***http://www.sti.nasa.gov***

- E-mail your question via the Internet to help@sti.nasa.gov

- Fax your question to the NASA Access Help Desk at 301–621–0134

- Telephone the NASA Access Help Desk at 301–621–0390

- Write to:
  NASA Access Help Desk
  NASA Center for AeroSpace Information
  7121 Standard Drive
  Hanover, MD 21076

NASA/TM—2005-213359

Estimation of ZnSe Slow-Crack-Growth Properties for Design of the Flow Enclosure Accommodating Novel Investigations in Combustion of Solids (FEANICS) Windows

Jonathan A. Salem
Glenn Research Center, Cleveland, Ohio

National Aeronautics and
Space Administration

Glenn Research Center

April 2005

Available from

NASA Center for Aerospace Information
7121 Standard Drive
Hanover, MD 21076

National Technical Information Service
5285 Port Royal Road
Springfield, VA 22100

Available electronically at http://gltrs.grc.nasa.gov

Estimation of ZnSe Slow-Crack-Growth Properties for Design of the Flow Enclosure Accommodating Novel Investigations in Combustion of Solids (FEANICS) Windows

Jonathan A. Salem
National Aeronautics and Space Administration
Glenn Research Center
Cleveland, Ohio 44135

Summary

This report reviews some of the literature on the fracture strength, fracture toughness, and crack growth properties of chemical-vapor-deposited ZnSe. The literature was reviewed to determine if the existing data on ZnSe is adequate to design windows for the Flow Enclosure Accommodating Novel Investigations in Combustion of Solids (FEANICS) project. Unfortunately, most of the published reports do not give all of the necessary design parameters despite having measured the data to do so. Further, the original data is not available. The data tabulated herein was determined by digitizing plots in original reprints of the publications. Based on the published data, an estimate of the slow-crack-growth parameters for small cracks in 100 percent humidity was made. For 100 percent humidity, the slow-crack-growth parameters for small crack (or single crystal) failure were estimated to be $n \leq 40$ and $A \geq 10^{20}$ m/s·(MPa $\sqrt{\text{m}}$)$^{-n}$. Weibull moduli estimated from bending of beams and circular plates ranged from 4 to 9, while fracture strengths ranged from 29 MPa in water to 72 MPa in dry nitrogen. Fracture toughness measurements ranged from 0.33 to 0.9 MPa $\sqrt{\text{m}}$, with the lower values representing failure from small flaws within grains and the larger values representing macroscopic cracks. Much of the data analyzed exhibited significant scatter, and the standard deviations were very large.

Introduction

The space station FEANICS (Flow Enclosure Accommodating Novel Investigations in Combustion of Solids) module contains eight 63-mm-diameter ZnSe windows that allow observation of various combustion experiments, as shown in figure 1. ZnSe is a soft, weak ceramic that exhibits crack growth in the presence of water. Further, it exhibits a large average grain size. This results in single grains dominating behavior by fracturing at energies lower than expected from macrocrack data. Thus hardware, such as a window fabricated from polycrystalline ZnSe, will contain large grains that fail at single-crystal fracture energies.

The design of fracture-critical components for the space station requires life analysis for conditions ranging from 40 to 90 percent relative humidity. In order to design windows sufficient to sustain the mission cycle, the literature on the fracture strength, fracture toughness, and crack growth properties of chemical-vapor-deposited (CVD) ZnSe was reviewed (refs. 1 to 11). Unfortunately, the publications have a tendency to give incomplete information both in terms of the data analysis and in terms of the experimental techniques used. Thus much of the data analyzed in this paper was digitized from plots in original publications, as the original data were not available.[1] This was necessary not only to get a

[1]Original data from references 1 and 2 were found to be unavailable per private communications with A.G. Evans, 2004, University of California, Santa Barbara, CA; S. Freiman, 2004, National Institute of Standards and Technology, Gaithersburg, MD; and J.J. Mecholsky, Jr., 2004, University of Florida, Gainesville, FL.

complete set of crack growth parameters for 100 percent humidity, but to determine the standard deviations.

The crack growth data reported herein is predominantly from two papers (refs. 1 and 2) because they contain the only available slow-crack-growth (SCG) data for ZnSe in water. Ideally, more documentation on how the data was generated and how the parameters were calculated should have been provided in these papers. This was especially the case for the single-crystal crack growth properties of ZnSe given in reference 2. In that case, the calculation method was not clearly provided, and the parameters were merely listed in a table. More disconcerting was the observation that both linear and nonlinear fits to the data plotted for polycrystalline ZnSe tested in air resulted in parameters in significant disagreement with those given in the paper. This did not appear to be a result of inaccurate digitization of the plot because digitization of the trend lines within the plots resulted in parameters in excellent agreement with those given in the paper.

Other complications with some of the data sets included significant scatter, relatively few data points, and the use of incorrect or unusual formulas for calculating the fracture energy. This was particularly the case for the reference 2 crack growth tests in water. The scatter was such that good parameter estimates could not be obtained.

Procedure

The data was digitized from original reprints or journal publications by using commercial software.[2] In most cases, the digitized data was plotted on the same scale and size as the original figure and overlaid on the original to determine that the process was accurate. Also, digitization was repeated several times for some plots and found to be very repeatable. However, it is acknowledged that the accuracy of the digitized data is limited by the accuracy of the original plots, which were made in the mid-1970s. Some reassurance is provided by the parameters reported in reference 3, which are in good agreement with those calculated herein.

For macrocrack data, the SCG parameters A and n of the equation

$$v = AK_{\mathrm{I}}^{n} \tag{1}$$

were determined from least squares linear regression of

$$\log\left(v\right) = n\log\left(K_{\mathrm{I}}\right) + \log\left(A\right) \tag{2}$$

where v is the crack velocity, K_{I} is the applied stress intensity factor, and A and n are the SCG parameters.

For the constant-displacement-rate data (i.e., "dynamic fatigue" data) of reference 1, the SCG parameters B and n as defined in reference 12

$$\sigma_f = \left[B\left(n+1\right)\sigma_i^{n-2}\dot{\sigma}\right]^{1/\left(n+1\right)} \tag{3}$$

were determined from linear regression of

$$\log\sigma_f = \frac{1}{n+1}\log\dot{\sigma} + \log D_d \tag{4}$$

[2]Un-Scan-It, Silk Scientific, P.O. Box 533, Orem, UT 84059.

where

$$\log D_d = \frac{1}{n+1}\log\left[B(n+1)\sigma_i^{n-2}\right] \tag{5}$$

and σ_f, $\dot{\sigma}$, and σ_i are the fracture strength, applied stress rate, and inert strength, respectively. For the static load data of reference 11, the SCG parameters B and n of

$$t_f = B\sigma_i^{n-2}\sigma_f^{-n} \tag{6}$$

were determined from linear regression of

$$\log t_f = -n\log\sigma_f + \log D_s \tag{7}$$

where

$$\log D_s = \log B + (n-2)\log\sigma_i \tag{8}$$

The SCG parameter A was calculated from

$$A = \frac{2K_{\mathrm{Ic}}^{2-n}}{BY^2(n-2)} \tag{9}$$

where K_{Ic} is the fracture toughness, and Y is the stress intensity factor coefficient. For optical components, an aspect ratio of $a/c = 0.1$ (where a = crack depth, and $2c$ = crack width) corresponding to a shallow surface crack is used for input to FLAGRO,[3] a fatigue crack growth program to analyze component life. This corresponds to $Y = 1.95$ where $K_{\mathrm{I}} = \sigma Y\sqrt{a}$ (ref. 12). In reference 2, Y was assumed to be 1.0 in calculation of the fracture toughness, and the formula used was unusual or incorrect. Thus the fracture energy and fracture toughness were recalculated as necessary for this report.

Results and Discussion

The digitized fracture strength and SCG data from figures 3, 4, and 6 of reference 1 are tabulated in tables I to III of this report, and the digitized data from figures 1 and 6 of reference 2 are tabulated in tables IV to VI. These data are also plotted in figures 2 to 5 on the original scales for comparison to the original publications. Fracture toughness values digitized from reference 7 are tabulated in table VII, and values from various reports are summarized in tables VIII and IX. Stress intensities calculated from the crack size data in table I of reference 11 are shown in figure 6 herein.

The results of least square fitting to the digitized data points in tables I to V for SCG in air and water are summarized in tables X and XI, respectively, and plotted in figures 7 to 13. Estimates of SCG parameters for small cracks in water are summarized in table XII and shown in figure 12. Standard deviations have been included in only a few cases because the data are either highly variable or represent

[3]NASA/FLAGRO 4.0.2, JSC 22267A, NASA Johnson Space Flight Center. See SSP 30560.

few data points. Weibull plots of the constant-displacement-rate data from figure 4 of reference 1 are shown in figure 14, and average strengths are summarized in figure 15.

Fracture Toughness

Macrocrack (i.e., where the crack is through hundreds of grains) fracture toughness values determined from double-cantilever beam (DCB), double torsion (DT), or precracked beam techniques ranged from a high of 0.9 MPa$\sqrt{\text{m}}$ in dry nitrogen to 0.62 MPa$\sqrt{\text{m}}$ in water (refs. 1, 2, and 9), as summarized in table VIII. Low-load Vickers indention cracks (100 g) resulted in 0.5 MPa$\sqrt{\text{m}}$ (ref. 10).

Small-crack (i.e., where the crack is through less than a few grains) estimates made from fractography of strength failures ranged from 0.22 to 0.49 MPa$\sqrt{\text{m}}$ for flaws ranging in size from 0.2 to 2.0 grains (ref. 7) (see table VII). The orientation of the failure plane with respect to the crystal structure was not determined. The test environment for these results was not distinguished in the original work (ref. 2), and fracture strength test results for both air and water were reported in the same paper. However, reference 7 indicates that the tests used to determine fracture toughness (likely most of the open and closed circles in figure 6 of reference 2, per J.J. Mecholsky, Jr., 2004, University of Florida, Gainesville, FL, private communication) were run in ~40 percent relative humidity (RH) air. Also, the original work did not consider the ellipticity of the crack in the analysis; however, it was considered in the second publication (ref. 7). The original publication (ref. 2) indicates a fracture toughness of 0.33 MPa$\sqrt{\text{m}}$, while the digitized data from the second (ref. 7) is in good agreement at 0.34±0.07 MPa$\sqrt{\text{m}}$. Evidently, reinterpretation of the data made little change in the average result.

Despite the good agreement between references 2 and 7, some reinterpretation of the single crystal fracture toughness estimation of reference 2 might be considered: (1) equation (3) of reference 2 is incorrect by a factor of $\sqrt{2}$ and Y was placed in the numerator, (2) plane stress was assumed, and (3) the assumed value of $Y = 1.0$ is not too accurate for the elliptical flaws observed. To determine if the errors in equation (3) were typos, the slope of the digitized data (see table VI) was estimated via linear regression with and without the intercept set to zero (ref. 2 forced a zero intercept). The estimated value via equation (3) of reference 2 was in good agreement with that reported (0.84 vs. 0.8 J/m^2), implying that equation (3) was used as shown and that digitization captured the data reasonably.

The common formulas

$$K_{\text{Ic}} = \sigma_f Y\sqrt{a} \quad \text{and} \quad 2\gamma_{\text{Ic}} = \frac{K_{\text{Ic}}^2}{E'} \tag{10}$$

where γ_{Ic} is the fracture surface energy, can be combined to give the fracture stress as a function of crack size:

$$\sigma_f = \frac{\sqrt{2E'\gamma_{\text{Ic}}}}{Y'} \cdot \frac{1}{\sqrt{a}} = b \cdot \frac{1}{\sqrt{a}} \tag{11}$$

where $E' = \dfrac{E}{1-\nu^2}$ for plane strain and $E' = E$ for plane stress, with E being the elastic modulus. Thus linear regression of σ_f versus $1/\sqrt{a}$ provides estimation of γ_{Ic} and K_{Ic} from the best-fit slope b:

$$\gamma_{Ic} = \frac{(bY)^2}{2E'} \tag{12}$$

and

$$K_{Ic} = bY \tag{13}$$

The values can also be estimated point wise via equation (10) and

$$\gamma_{Ic} = \frac{(\sigma_f Y)^2 a}{2E'} \tag{14}$$

Use of equations (12) and (13) to estimate the fracture energy and fracture toughness requires the crack dimensions. Unfortunately, only the minor axis lengths were reported in reference 2. Thus the fracture energy and fracture toughness values via equations (12) and (13) are summarized in table IX for various crack shapes. The possible plane strain values range from 0.6 to 1.45 J/m^2 for fracture energy and 0.30 to 0.47 MPa$\sqrt{\text{m}}$ for fracture toughness for typical Y values. For the case assumed in reference 2, the calculated fracture energy is about one-half that reported; however, it is fortuitous that the actual energy and fracture toughness are similar to or higher than that reported in reference 2 because the error in Y nominally canceled with the $\sqrt{2}$ error ($Y \geq 1.26$). This may explain why reinterpretation of the original data with a more accurate approach (ref. 7) did not change the estimated fracture toughness.

Pointwise estimates made with equations (10) and (14) gave similar results. Fitting without forcing the intercept to zero resulted in an intercept of 12 MPa and significantly lower fracture energies and toughness values (b = 0.17).

The static fatigue data in table I of reference 11 provides an opportunity to estimate the nominal, initial stress intensity sustained during constant-stress testing of CVD ZnSe in 50 percent RH air at 47 to 56 MPa. The calculated stress intensities range from 0.13 to 0.38 MPa$\sqrt{\text{m}}$ (averaging 0.25 ± 0.09 MPa$\sqrt{\text{m}}$), and the specimens that failed on loading exhibit stress intensities greater than 0.24 MPa$\sqrt{\text{m}}$. The stress intensities show little dependence on the time to failure, however, the expected dependence on crack size was exhibited (the maximum stress intensity usually occurred at the maximum crack depth, a), as shown in figure 6. For crack widths 2c greater than ~50 μm, the initial stress intensities compare to the small crack value reported (0.33 MPa$\sqrt{\text{m}}$) in references 2 and 7. Also, it was reported (ref. 11) that the critical flaw size calculated with the measured stress and a "single crystal fracture toughness" of ≈0.5 J/m^2 gave good agreement with the observed boundaries of time-dependant intergranular failures, implying that the intergranular fracture toughness for small cracks, as calculated via equation (10), is at least 0.26 MPa$\sqrt{\text{m}}$. Thus, for the sake of simplicity, K_{Ic} will be taken as ~0.33 MPa$\sqrt{\text{m}}$ for failure from small cracks of intergranular or transgranular nature.

The large difference between the small-crack and macrocrack values (0.33 and 0.6 to 0.9 MPa$\sqrt{\text{m}}$, respectively) is likely due to (1) single crystal effects and (2) grain bridging resulting from the coarse grain size of ZnSe. The relevance of the single crystal values to FEANICS can be determined from the stress levels expected and the grain size of the ZnSe to be used. The average grain size from several measurements normal and parallel to the growth direction in CVD ZnSe produced by Raytheon ranged from 45 to 60 μm (refs. 3 and 9), and those for Gould and Coors were much larger (190 and 435 μm, respectively) (ref. 9). Unfortunately, the standard deviations of the measurements were not reported. The critical flaw size $a_{critical}$ for the FEANICS windows (applied stress $\sigma \approx 10$ MPa, $K_{Ic} \approx 0.33$ MPa$\sqrt{\text{m}}$) can be determined by rearrangement of equations (10) or (11) and by setting σ to σ_f:

$$a_{\text{critical}} = \left(\frac{K_{\text{Ic}}}{Y\sigma_f} \right)^2 \tag{15}$$

or

$$a_{\text{critical}} = \left(\frac{b}{\sigma_f} \right)^2 \tag{16}$$

For Y between 1.26 (a/c = 1.00) and 1.95 (a/c = 0.1), equation (15) indicates that the critical crack is between 685 and 285 μm, or about 5 to 10 times the average grain size for current CVD ZnSe (ref. 10) as shown in figure 16. However, the lack of information on both the gain size distribution and the minimum crack length for macrocrack fracture toughness precludes strong conclusions regarding the possibility of failure at single crystal fracture energies. Potentially, failure could occur from a very large grain or several large grains of similar orientation. Thus the design should be based on small-crack properties.

Slow-Crack-Growth Parameters

Fits to the data in reference 1 resulted in n values in reasonable agreement with those reported; however, no values for A were reported. Analysis of the constant-displacement-rate data generated by point loading circular plates supported by three balls (B–O–3B) resulted in reasonable agreement with fits to DT test data (n = 50.3±32 and $A = 9.97\times10^3$ m/s·(MPa $\sqrt{\text{m}}$)$^{-n}$ versus n = 39.6 and $A = 1.09\times10^3$ m/s·(MPa $\sqrt{\text{m}}$)$^{-n}$, respectively); however, the standard deviations were very large, and the correlation was low, as shown in figure 7. The SCG parameters derived from the constant-displacement-rate data are relatively sensitive to the fracture toughness value used in equation (9). If a single crystal estimate of K_{Ic} = 0.33 MPa $\sqrt{\text{m}}$ is used, then A increases substantially to $A_{\text{Single}} = 1.08\times10^{25}$ m/s·(MPa $\sqrt{\text{m}}$)$^{-n}$ in water, a value more conservative than that estimated in reference 2 for single crystal failure in air.

Fits to the air data of reference 2 resulted in somewhat different parameters than reported in table I of reference 2 (n = 24.7 vs. n = 40, see table X and figure 8 herein). However, fits to the line drawn on figure 1 of reference 2 were in excellent agreement with table I of reference 2 (n = 39.6 vs. n = 40). No description of how the data lines were estimated is given in reference 2. Because the digitization technique appears to be accurate and fits to the line agree with the reported values, the source of discrepancy is unclear. The value of n = 40 may have been assumed based on the results of reference 1.

Attempts to fit the water data of reference 2 were complicated by the large amount of scatter in the measured stress intensity and the small number of data points at larger crack velocities, as shown in figures 9 and 10. The regression coefficient was very poor (r^2 = 0.22), and the parameters listed in table XI for all 21 data points are not very meaningful. A final attempt to get parameters from the data was made by truncating the large-stress-intensity, low-velocity values in figure 10. These outlying values may have resulted from crack pinning by large grains. The truncated data set is plotted in figures 11 and 12, and linear regression indicates n = 24.6, A = 282 m/s·(MPa $\sqrt{\text{m}}$)$^{-n}$, and r^2 = 0.90. The curves shown in figures 10 and 11 are nonlinear fits to the data and result in lower n and A values.

It is notable that reference 3 reports a least squares fit to the DT data in figure 6 of reference 1 (fig. 4 herein). The parameters reported in reference 3 were n = 39.9 and A = 1202 m/s·(MPa $\sqrt{\text{m}}$)$^{-n}$, in good agreement with the values determined in this work via digitization and regression (see table XI: n = 39.6, $A = 1.09\times10^3$ m/s·(MPa $\sqrt{\text{m}}$)$^{-n}$), implying that the digitization process used herein is reasonably accurate.

Also, the data in figure 1 of reference 2 were plotted in reference 3 and indicate slopes in agreement with those estimated in this report.

Some static and cyclic loading of CVD ZnSe in air has been performed (refs. 3, 9, and 11). Unfortunately the statistical significance is low due to the scatter and the number of runouts in the data sets as shown in figure 13. Regression of the data in references 3 and 11, which is identical, resulted in $n = 21 \pm 6$ and $A = 4.82 \times 10^{-6}$ with a regression coefficient of $r^2 = 0.35$. Fractographic analysis of the test specimens indicated that time-dependant failures occurred from intergranular growth regions surrounding small machining flaws (2 to 20 μm), whereas fast fracture occurred in a transgranular manner from machining flaws within large grains. Analysis of the data (ref. 11) indicated that single crystal parameters gave a somewhat better estimate of the life of the test specimens than polycrystalline parameters.

The single crystal parameter $A_{\text{Single}} = 1.8 \times 10^{18}$ m/s·(MPa $\sqrt{\text{m}}$)$^{-n}$ of reference 2 for air was reported to have been derived (1) by assuming that the slopes of the polycrystalline (macrocrack) and single crystal SCG curves were the same and (2) by using the data in figure 1 of that article. The value was likely derived by equating the velocity equation to itself at fracture and solving for A:

$$v = A_{\text{Poly}} K_{\text{Ic Poly}}^{n} = A_{\text{Single}} K_{\text{Ic Single}}^{n} \tag{17}$$

so that

$$A_{\text{Single}} = A_{\text{Poly}} \left(\frac{K_{\text{Ic Poly}}}{K_{\text{Ic Single}}} \right)^{n} \tag{18}$$

This assumes that the velocities at fracture are equal for the single crystal case and the polycrystalline case. Calculation with the nominal values provided in the text ($K_{\text{Ic Poly}} = 0.90$ MPa $\sqrt{\text{m}}$, $K_{\text{Ic Single}} = 0.33$ MPa $\sqrt{\text{m}}$, $n = 40$, and $A_{\text{Poly}} = 2.0$ m/s·(MPa $\sqrt{\text{m}}$)$^{-n}$) gives $A_{\text{Single}} = 5.4 \times 10^{17}$ m/s·(MPa $\sqrt{\text{m}}$)$^{-n}$, in good agreement considering the sensitivity of equation (18) to small changes in the input values. Equation (18) can also be used to estimate an A_{Single} value for water from the data sets in references 1, 2, and 11. Table XII summarizes single crystal parameter estimates made with equation (18) for the DT and DCB methods and with equation (9) for the constant-displacement-rate data and constant-stress data. It should be noted that equation (9) implies a power of $(n - 2)$, relating single crystal and polycrystalline values under the assumption that B remains constant:

$$A_{\text{Single}} = A_{\text{Poly}} \left(\frac{K_{\text{Ic Poly}}}{K_{\text{Ic Single}}} \right)^{n-2} \tag{19}$$

Thus the use of equation (18) to shift constant-displacement- or any strength-based data provides different results than the direct approach of using equation (9).

Fracture Strength and Weibull Modulus

Weibull moduli for ZnSe were estimated from the digitized data of figure 4 in reference 1 (constant-displacement-rate data on circular plates under B–O–3B loading). Weibull plots of the data are shown in figure 14 and the estimated Weibull moduli ($m = 4$ to 6) are summarized in table II. The mean fracture strength ranged from 56.1±10.1 MPa in water to 71.6±17.3 MPa in dry nitrogen (where the ± values are

one standard deviation). The dimensions of the test specimens and the load fixture were not given, and thus the effective areas cannot be estimated.

Results for three- and four-point flexure test specimens were reported in reference 2. The measured fracture strengths were 29±5 MPa for water and 40±4 for air (where the ± values are the 95 percent confidence limits). The three-point test specimens, though polished on the tensile face, were the arms of the DCB tests. Thus the uniaxial flexure values may be lower than the B–O–3B results because of polishing differences and edge effects.

Testing at AFML[4] in the mid-70s resulted in average four-point bend strengths ranging from 27 to 56 MPa and Weibull moduli ranging from 6 to 9 (refs. 3 and 9), depending on the quality of surface polish and edge finish. Once rounded and polished edges were employed, strengths improved (>50 MPa). Weibull analysis of 139 four-point bend tests indicate a Weibull modulus of $m = 9.23$, a characteristic strength of 54.3 MPa, and a scale parameter of 104.1 MPa·mm$^{2/m}$ (or 23.3 MPa·m$^{2/m}$). The test specimens were larger than typically used to test ceramics, and thus a large effective area of $A_e = 405$ mm^2 resulted. The average strength was 52.3±6.9 MPa.

Note that measured "strength" of dense optical materials is usually controlled to a significant extent by the surface flaws introduced during grinding, polishing, and handling. Better polishing usually results in higher fracture strength, and the strength is a function of the area and/or volume under stress as governed by Weibull statistics. However, it has been reported by Miles (ref. 13) that the strength of CVD ZnSe[5] depends only weakly on the volume of material under stress and "only slightly on the degree of perfection of the surface polish." The main factor influencing fracture strength is grain size: For grain sizes of 25, 53, and 400 μm, Miles reported strengths of 67, 53, and 32 MPa, respectively. No details on the test method or environment were reported. Miles concluded that the incipient flaw size is comparable to the grain size (typically 50 to 100 μm) (ref. 13). Reference 2 reported that "occasionally fracture occurred from a region containing several small pores." Thus failure from within the volume cannot be ruled-out. Unfortunately, no statistics for such failures are available.

In addition to the dependence of fracture strength on grain size, it should be kept in mind that ZnSe is relatively soft (Knoop hardness of HK ≅ 1.4, 1.0, and 0.3 GPa for grain sizes of 25, 51, and 400 μm (refs. 13 and 3)) and has low toughness; thus it is easily damaged. As a result, the strength can be easily and immediately reduced by poor handling. Ideally, any strength measurements used in the design process should be generated on specimens polished and handled identically to the components being designed, and appropriate reductions for service damage should be considered.

The elastic modulus and Poisson's ratio as measured via strain gages were 72.4 GPa and 0.30, respectively (ref. 9). Reference 2 reported an elastic modulus of 69 GPa, though no source was cited.

Conclusions

Based on 1970s vintage data for ZnSe, the parameters for design of applications exposed to high humidity—as in the windows for the Flow Enclosure Accommodating Novel Investigations in Combustion of Solids (FEANICS) module discussed herein—are $n \le 40$, $A_{single} \ge 10^{20}$ m/s·(MPa$\sqrt{\text{m}}$)$^{-n}$, and $K_{Ic} \le 0.33$ MPa$\sqrt{\text{m}}$. The slow-crack-growth parameters for macrocracks in water are much different: n is between 25 and 80 and A is ~1000. The only crack growth data for small flaws was generated by constant-displacement-rate testing or constant-stress testing of smooth sections containing grinding and polishing flaws. If the single-crystal fracture toughness is used to estimate A_{Single} from the constant displacement rate test data or to shift macroscopic v-K_I curves via equation (18), A_{Single} ranges from 10^{20} to 10^{25} m/s·(MPa$\sqrt{\text{m}}$)$^{-n}$ for water. For the same dynamic fatigue test data, the analysis herein indicates that n was 50.3, the Weibull parameter m ranged from 4 to 7, and the characteristic fracture strength

[4]Air Force Materials Laboratory, Wright-Patterson Air Force Base, OH, 45433.
[5]The material was likely Raytran CVD ZnSe. At that time, Raytran was produced by Raytheon Company, Waltham, MA.

ranged from 52 MPa in water to 78 MPa in dry nitrogen. The standard deviations on the slow-crack-growth parameters were very large.

Recommendations

(1) In addition to the design code FLAGRO (NASA/FLAGRO 4.0.2, NASA Lyndon B. Johnson Space Center, Houston, TX), Weibull-based life prediction methods should be considered for designing components from ZnSe. The approach does not require estimation of the fracture toughness or the parameter *A*, but only the parameter *B*. The parameter *B* should be estimated statistically from smooth sections tested either statically or dynamically at stress levels that allow failure from real, small flaws that have similitude with those in the component being designed. Proof testing and appropriate safety factors or confidence intervals would still be required.

(2) For design of ZnSe components with FLAGRO, the single crystal crack growth parameters and fracture toughness values should be used.

(3) Ideally, better data on ZnSe should be generated. The DT data discussed and analyzed in this report is the most repeatable; however, it is based on macroscopic crack growth. The dynamic fatigue data analyzed in this study sampled real, small flaws in ZnSe. However, the statistical significance is weak due to the small sample size used (18 tests in water). A sample size of 40 is required by the current standard for estimating slow-crack-growth parameters (ASTM C 1368–01). At a minimum, fracture strength data should be generated on test specimens prepared identically to the windows. Better fatigue data would be beneficial; however, it needs to be generated in conjunction with fractography to determine the frequency of failure from single grains or intergranular regions. This would allow lifetime design for intergranular failure and fast fracture failure from single crystals. However, it would be somewhat time consuming. At the same time, the effect of scale on fracture strength, which has been reported to be small, should be measured in order to determine the necessity of Weibull statistics for ZnSe component design.

(4) Because ZnSe is relatively soft, an investigation of the strength loss due to handling damage might be considered.

References

1. Evans, A.G.; and Johnson, H.: Fracture-Mechanics Study of ZnSe for Laser Window Applications. J. Amer. Ceram. Soc., vol. 58, nos. 5–6, 1975, pp. 244–249.
2. Freiman, S.W., et al.: Influence of Microstructure on Crack Propagation in ZnSe. J. Am. Ceram. Soc., vol. 58, nos. 9–10, 1975, pp. 406–409.
3. Graves, G.A.; McCullum, D.E.; and Wimmer, J.M.: Exploratory Development and Investigation of the Thermal, Electrical, Mechanical, and Physical Properties of Infrared Laser Window and I–R Transmitting Materials; Final Technical Report. AFML–TR–77–23, UDRI–TR–77–06, 1977. Available from the NASA Center for Aerospace Information.
4. Iden, D.J.; Detrio, J.A.; and Fox, J.: Optical Window Mechanical Strength and Reliability; Interim Report. AFWAL–TR–83–4059, UDR–TR–83–73, 1983. Available from the NASA Center for Aerospace Information.
5. Taylor, R.L.; and Goela, J.S.: Specification of Infrared Optical Materials for Laser Applications. Proceedings of the SPIE—The International Society for Optical Engineering, vol. 607, 1986, pp. 22–35.
6. Fernelius, Nils C.; Graves, George A.; and Knecht, Walter L.: Characterization of Candidate Laser Window Materials. Emerging Optical Materials, vol. 297, 1981, pp. 188–195.

7. Rice, R.W.; Freiman, S.W.; and Mecholsky, J.J., Jr.: The Dependence of Strength-Controlling Fracture Energy on the Flaw-Size to Grain-Size Ratio. J. Am. Ceram. Soc., vol. 63, nos. 3–4, 1980, pp. 129–136.
8. Cargo Bay Door IR Window Reliability Analysis. BDM International, Inc., Report BDM/ABQ–92–0056–TR, 1992.
9. Wurst, J.C.; and Graham, T.P.: Thermal, Electrical, and Physical Measurements of Laser Window Materials; Final Report. AFML–TR–75–28, UDRI–TR–75–06, 1975. Available from the NASA Center for Aerospace Information.
10. CVD Zinc Selenide. Rohm and Haas Advanced Materials data sheet, ZnSe Rev. 1, May 2000.
11. McKinney, K.R.; Mecholsky, J.J.; and Freiman, S.W.: Delayed Failure in Chemically Vapor Deposited ZnSe. J. Am. Ceram. Soc., vol. 62, nos. 7–8, 1979, pp. 336–340.
12. Ritter, J.E., Jr.: Engineering Design and Fatigue Failure of Brittle Materials. Fracture Mechanics of Ceramics. R.C. Bradt, D.P.H. Hasselman, and F.F. Lange, eds., Plenum Press, New York, NY, 1978, pp. 667–686.
13. Miles, P.: High Transparency Infrared Materials—A Technology Update. Opt. Eng., vol. 15, no. 5, 1976, pp. 451–459.

TABLE I.—CRACK VELOCITY OF ZnSe IN WATER AND AIR
[Digitized from the lines in fig. 3 of ref. 1.[a]]

Water		Air	
Stress intensity, MPa $\sqrt{m}$	Crack velocity, m/s	Stress intensity, MPa $\sqrt{m}$	Crack velocity, m/s
Upper bound			
0.661	8.637×10^{-7}	0.732	6.636×10^{-7}
.674	5.897×10^{-6}	.748	3.290×10^{-6}
.691	7.176×10^{-5}	.780	7.397×10^{-5}
.709	8.811×10^{-4}	.799	4.540×10^{-4}
Lower bound			
0.603	1.105×10^{-6}	0.684	7.981×10^{-7}
.616	6.840×10^{-6}	.699	3.922×10^{-6}
.637	1.407×10^{-4}	.724	4.903×10^{-5}
.654	1.200×10^{-3}	.749	5.658×10^{-4}

[a]Upper and lower bounding lines of shaded area were digitized. Original data sets were generated with double torsion and double cantilever beam testing and fit by least squares linear regression.

TABLE II.—FRACTURE STRENGTH OF ZnSe
[Digitized from data points in fig. 4 of ref. 1.]

Statistics[a]	Fracture strength,[b] σ_f, MPa			
	Water		Air	Dry N_2
	Stress rate			
	0.075 MPa/s	75 MPa/s	0.075 MPa/s	75 MPa/s
Failure probability				
0.10	34.92	42.63	45.45	47.58
0.20	39.26	47.18	48.57	52.98
0.30	46.15	48.07	52.96	56.63
0.40	46.24	51.66	56.02	67.77
0.50	50.42	56.69	58.50	68.76
0.60	51.68	58.96	61.46	76.71
0.70	53.46	61.01	68.88	87.54
0.80	56.53	63.01	77.10	90.23
0.90	62.94	75.96	88.19	96.21
Mean strength,[c] MPa	49.1±8.6	56.1±10.1	61.9±13.9	71.6±17.3
Weibull[d] modulus, *m*	6.1	6.5	5.4	4.5
Characteristic strength, σ_θ MPa	52.6	60.0	66.8	78.2

[a]Statistics were calculated from digitized data.
[b]Data was generated via constant-displacement-rate testing of circular plates supported on three balls and loaded with one ball (B–O–3B configuration).
[c]Values after ± are one standard deviation.
[d]Estimated with rank regression. Estimates via maximum likelihood estimator are shown in legend of fig. 14.

TABLE III.—CRACK VELOCITY OF ZnSe IN WATER
[Digitized from data in fig. 6 of ref. 1.[a]]

Stress intensity, MPa $\sqrt{m}$	Crack velocity, m/s
0.594	1.009×10^{-6}
.602	1.331
.599	1.704
.602	2.591
.613	2.574
0.606	3.548×10^{-6}
.615	4.710
.613	6.411
.626	8.563
.624	1.158×10^{-5}
0.641	1.255×10^{-5}
.630	1.828
.642	1.676
.654	2.456
.637	2.695
0.649	3.029×10^{-5}
.648	5.147
.651	6.834
.654	9.130
.664	8.271
0.670	9.889×10^{-5}
.678	1.485×10^{-4}
.667	1.523
.670	2.111
.673	2.587

[a]Data generated via double torsion testing in water.

TABLE IV.—CRACK VELOCITY OF ZnSe IN WATER AND AIR
[Digitized from data points in fig. 1 of ref. 2.[a]]

Water		Air (40 to 50% RH)[b]	
Stress intensity, (MPa $\sqrt{m}$)	Crack velocity, m/s	Stress intensity, MPa $\sqrt{m}$	Crack velocity, m/s
0.548	3.007×10^{-8}	0.614	1.990×10^{-8}
.423	4.347	.658	4.210×10^{-8}
.404	4.773	.638	1.410×10^{-7}
.505	6.477	.678	2.000×10^{-7}
0.498	1.494×10^{-7}	0.740	9.880×10^{-7}
.473	2.967	.724	1.080×10^{-6}
.480	3.533	.665	1.090×10^{-6}
.438	3.904	.751	3.000×10^{-6}
0.513	4.103×10^{-7}	0.696	4.910×10^{-6}
.540	4.735	.717	6.870×10^{-6}
.459	9.061	.757	9.040×10^{-6}
.494	9.886		
0.555	1.473×10^{-6}		
.474	1.915		
.542	2.681		
.449	4.255		
0.560	5.459×10^{-6}		
.485	2.010×10^{-5}		
.520	4.935×10^{-5}		
.555	9.921×10^{-5}		
.569	1.442×10^{-4}		

[a]Data was generated via double cantilever beam testing.
[b]Figure 1 of ref. 2 indicated 50 percent relative humidity (RH), whereas text indicated ~40 percent RH.

TABLE V.—CRACK VELOCITY OF ZnSe IN WATER AND AIR
[Digitized from the lines in fig. 1 of ref. 2.[a]]

Water		Air	
Stress intensity, MPa $\sqrt{m}$	Crack velocity, m/s	Stress intensity, MPa $\sqrt{m}$	Crack velocity, m/s
0.464	1.432×10^{-8}	0.622	1.353×10^{-8}
.496	5.746×10^{-7}	.657	1.142×10^{-7}
.525	1.391×10^{-5}	.708	2.223×10^{-6}
.559	4.062×10^{-4}	.767	5.587×10^{-5}

[a]Method used to generate lines was not described in ref. 2.

TABLE VI.—FRACTURE STRENGTH OF ZnSe
[Digitized from data points in fig. 6 of ref. 2.]

Fracture strength, MPa	Inverse of square root crack length, $(\sqrt{m})^{-1}$	Crack length,[a] μm
24.3	106	89
36.1	112	80
32.9	119	71
31.4	141	50
28.9	141	50
26.7	158	40
26.8	160	39
25.9	161	39
35.8	95	110
30.0	179	31
34.0	160	39
37.5	158	40
40.6	160	39
45.1	140	51
47.7	161	39
42.9	172	34
50.3	179	31
58.8	159	40
56.0	189	28
54.9	222	20
50.5	219	21
48.1	221	20
47.9	223	20
Mean values		
39.7±10.6	162±36	44±23

[a]Crack lengths correspond to minor axis.

TABLE VII.—FRACTURE TOUGHNESS OF ZnSe IN AIR

[Digitized from data points in fig. 6 of ref. 7.[a]]

Flaw size to grain size ratio	Fracture toughness, MPa $\sqrt{m}$	Fracture energy, J/m^2
1.002	0.223	1.477
.992	.280	1.313
.294	.265	1.187
.300	.286	1.041
.047	.287	.970
.407	.489	.947
.209	.452	1.139
.285	.422	.947
.401	.382	.741
.593	.361	.616
.199	.333	.705
.204	.317	.756
.315	.323	.762
.411	.311	.837
.987	.354	.883
1.993	.354	.857
1.988	.409	.823
Mean values		
0.62±0.59	0.34±0.07	0.94±0.23

[a]Values estimated from fractography of strength specimens tested in air via three-point bending.

TABLE VIII.—FRACTURE TOUGHNESS OF ZnSe TESTED IN AIR AND WATER

Data source	Test method[a]	Fracture toughness, MPa $\sqrt{m}$
Macrocrack data		
Ref. 1, text	DT and DCB, dry N_2	0.9
Ref. 2, text	DCB, Air (40 to 50 percent RH)	0.7
Ref. 2, text	DCB, water	0.62
Ref. 9, table 9	Notched and cracked beam[b]	0.68±0.04
Small-crack data		
Ref. 2, table 1	Fractography/strength tests	0.33
Ref. 7, figure 6 data points	Fractography/strength tests	[c]0.34±0.07 (17)
Ref. 10, commercial data sheet	100-g indentation	0.5
Ref. 11, analysis of data in table I	Fractography of constant-stress tests	[d]0.25±0.09 (17)

[a]DT is double torsion and DCB, double-cantilever beam. RH is relative humidity.

[b]Specific test environment was not reported, but most of the data in this report appears to have been generated in 50 percent RH laboratory air.

[c]Average and standard deviation of 17 data points, digitized from fig. 6 of ref. 7. Same data as reported in table 1 of ref. 2. Reference 7 reported that tests were run in 40 percent RH air. Data was scanned to determine standard deviation. See table VII of this report for individual values.

[d]Initial stress intensity sustained.

TABLE IX.— FRACTURE ENERGY AND FRACTURE TOUGHNESS OF ZnSe FOR VARIOUS STRESS INTENSITY FACTOR COEFFICIENTS *Y*
[Estimated from eqs. (12) and (13) using data from table VI with E = 69 GPa, v = 0.31, and b = 0.24]

Stress intensity factor coefficient, *Y*	Fracture energy, γ_{Ic}, J/m^2		Fracture toughness, K_{Ic}, MPa $\sqrt{\text{m}}$
	Plane stress	Plane strain	
1.00 (ref. 2)	0.38	0.42	0.24
1.26 (semicircular)	.60	.67	.30
$\sqrt{\pi}$ (center-cracked panel)	1.19	1.32	.43
1.95 (a/c = 0.1)	1.45	1.60	.47

TABLE X.—SLOW-CRACK-GROWTH PARAMETERS FOR ZnSe IN AIR
[Estimated from data in tables I, IV, and V, and as reported in refs. 1, 2, and 11.]

Data source	Test conditions,[a] air	Crack-growth parameters	
		A, m/s·(MPa $\sqrt{\text{m}}$)$^{-n}$	n[b]
Ref. 1, line on figure 3[c]	DT and DCB	7.4×10^{5}	72
Ref. 2, 11 data points on figure 1	DCB	[d]6.2×10^{-3}	24.7±5.6
Ref. 2, line on figure 1	DCB	2.0	39.6
Ref. 2, table 1	DCB	2.0	40
Ref. 2, table 1	----------	1.8×10^{18}	40
Ref. 11, table 1[e]	four-point, static	4.82×10^{-6}	20.7±5.5

[a]DT is double torsion and DCB, double-cantilever beam.
[b]Value after ± is one standard deviation.
[c]Lower bound line of shaded region shown in figure.
[d]Estimated standard deviation of log(A) via linear regression of eq. (2) is 0.90.
[e]Value of 0.9 MPa $\sqrt{\text{m}}$ was used in estimating A from eq. (9). If the single crystal estimate of fracture toughness from ref. 2 is used, then A = 646.

TABLE XI.—SLOW-CRACK-GROWTH PARAMETERS *A* AND *n* FOR ZnSe IN WATER
[Estimated from data in tables I to V and as reported in refs. 1 and 2.]

Data source	Test method[a]	A, m/s·(MPa $\sqrt{\text{m}}$)$^{-n}$	n
Ref. 1, line on figure 3[c]	DT and DCB	1.11×10^{13}	86.4
Ref. 1, text	DT and DCB	Not reported	45 to 80
Ref. 1, figure 4, 18 data points[d]	B–O–3B, dynamic	9.98×10^{3}	50.3±32
Ref. 1, 25 data points on figure 6	DT	[e]1.09×10^{3}	39.6±2.0
Ref. 2, 21 data points on figure 1	DCB	[f]5.0×10^{-3}	12.0±5.1
Ref. 2, 9 of 21 data points on figure 1	DCB	282	24.6
Ref. 2, line on figure 1	DCB	3.61×10^{10}	55.1

[a]DT is double torsion; DCB, double-cantilever beam; and B–O–3B, point loading of circular plates supported by three balls.
[b]Value after ± is one standard deviation.
[c]Lower bound line of shaded region shown in figure.
[d]Value of 0.9 MPa $\sqrt{\text{m}}$ was used in estimating *A*. If single crystal estimate of fracture toughness from ref. 2 is used, then $A = 1.08\times10^{25}$. See table XII.
[e]Estimated standard deviation of log(A) via linear regression of eq. (2) is 0.397. Reference 3 gives 0.441.
[f]Estimated standard deviation of log(A) via linear regression of eq. (2) is 1.57.

TABLE XII.—SLOW-CRACK-GROWTH PARAMETERS FOR SMALL CRACKS (SINGLE CRYSTAL FAILURE) FOR ZnSe IN WATER
[Estimated from data in tables I to V and eq. (9) or (18).]
[Fracture toughness of K_{Ic} = 0.33 MPa $\sqrt{\text{m}}$ was used.]

Data source	Test method,[a] water	Crack growth parameters	
		A_{Single}, m/s·(MPa $\sqrt{\text{m}}$)$^{-n}$	n
Ref. 1, line on figure 3[b]	DT and DCB	5.05×10^{50}	86.4
Ref. 1, data points on figure 4	B–O–3B, dynamic[c]	1.08×10^{25}	50.3
Ref. 1, data points on figure 6	DT	1.97×10^{20}	39.6
Ref. 2, data points on figure 1	DCB	8.61×10^{2}	12.0
Ref. 2, truncated data of figure 1	DCB	1.46×10^{13}	24.6

[a]DT is double torsion; DCB, double-cantilever beam; and B–O–3B, point loading of circular plates supported by three balls.
[b]Lower bound line of shaded region shown in figure.
[c]Equation (9) used to estimate parameter *A*.

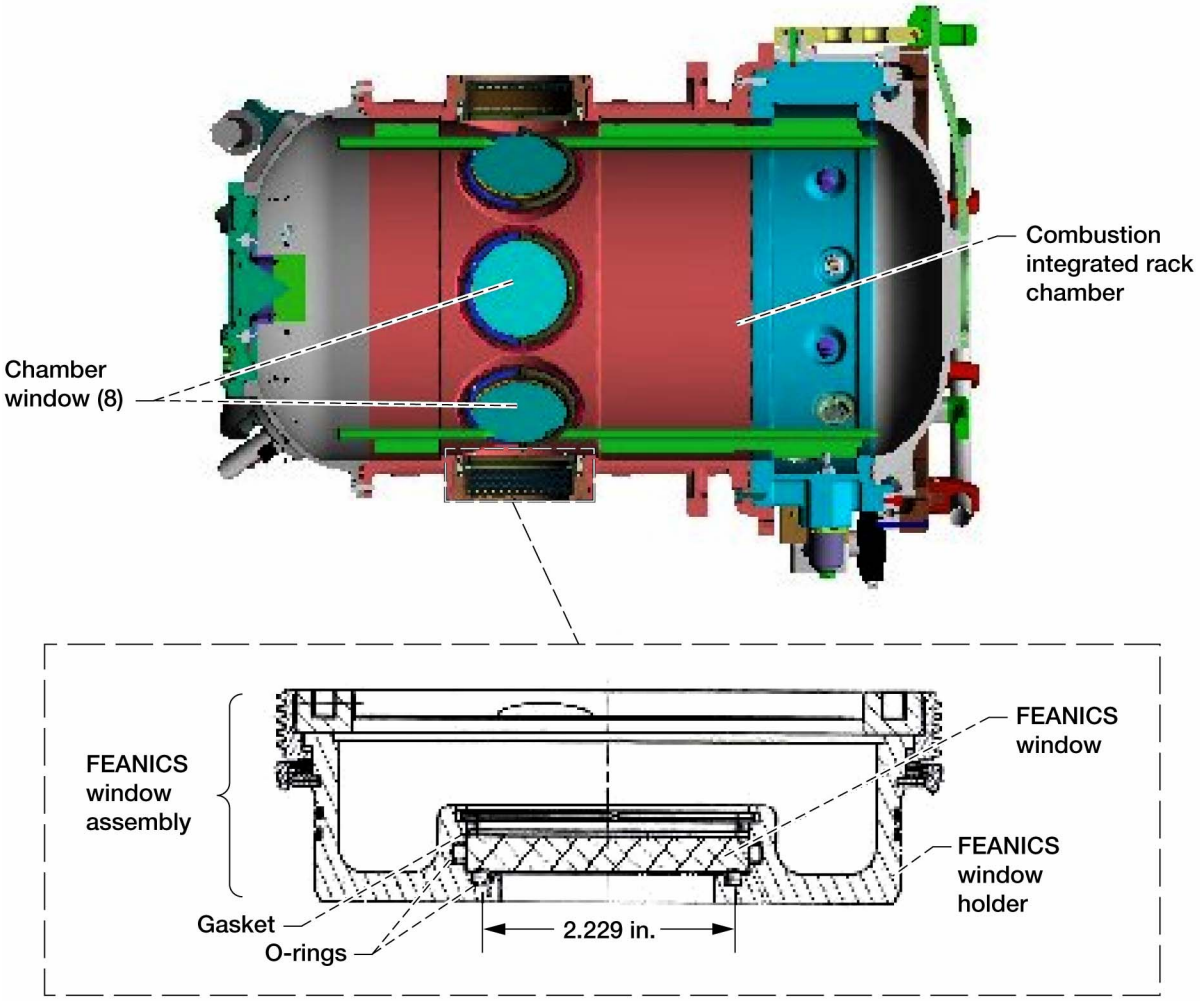

Figure 1.—Flow Enclosure Accommodating Novel Investigations in Combustion of Solids (FEANICS) module and ZnSe window assembly.

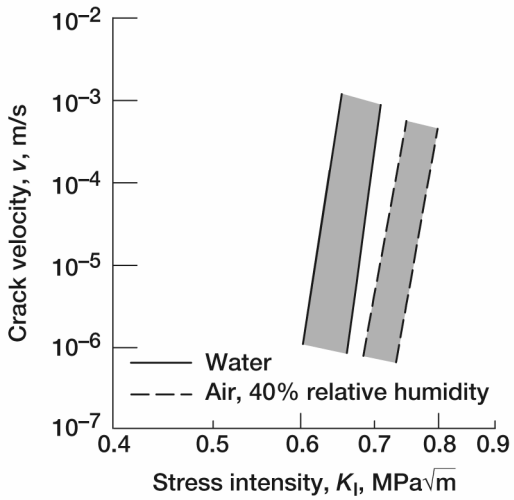

Figure 2.—Crack velocity *v* as function of stress intensity factor K_I for ZnSe in water and air. Data is from table I and plotted on the scale used in original publication.

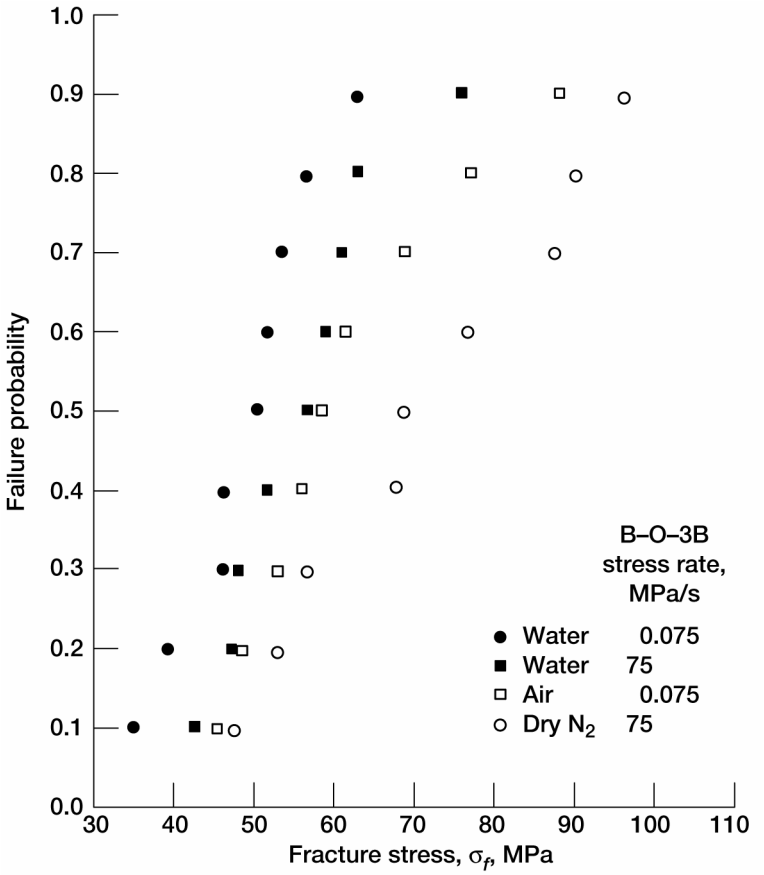

Figure 3.—Fracture stress σ_f as function of probability of failure for polished ZnSe disks in water, air, and dry nitrogen. Data is from table II and plotted on the scale used in original publication. B–O–3B is point loading of circular plates supported by three balls.

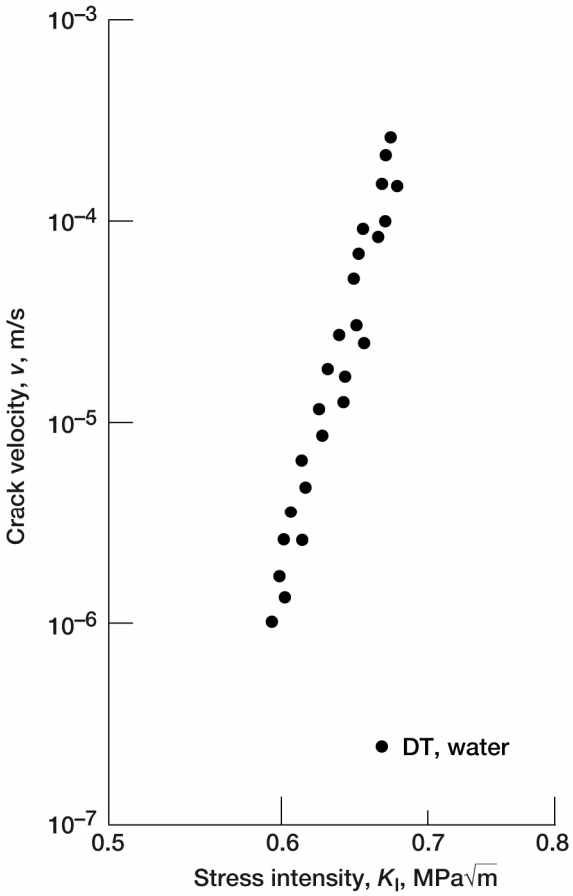

Figure 4.—Crack velocity v as function of stress intensity factor K_I for ZnSe in water. Data is from table III and plotted on the scale used in original publication. DT is double torsion.

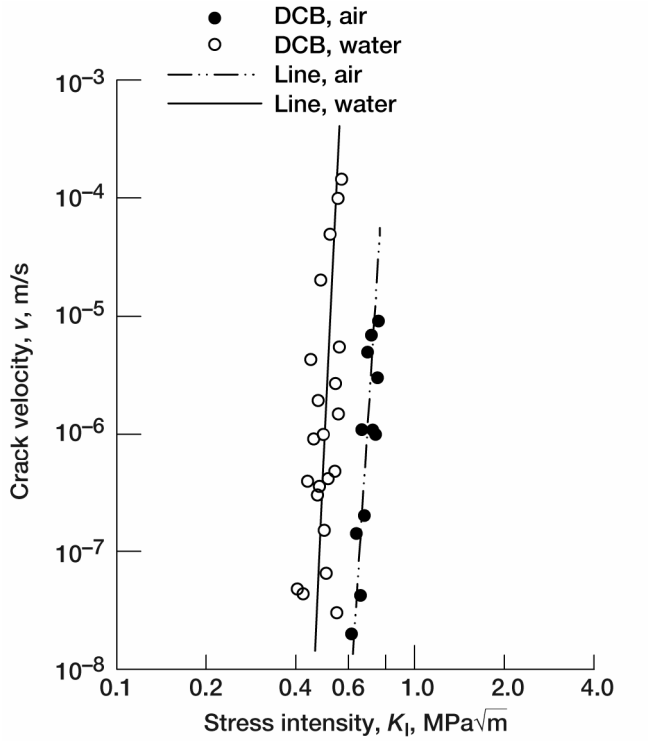

Figure 5.—Crack velocity *v* as function of stress intensity factor K_I for ZnSe in water and air. Data is from table IV. Lines are from table V. Both data points and lines are plotted on the scale used in original publication. DCB is double-cantilever beam.

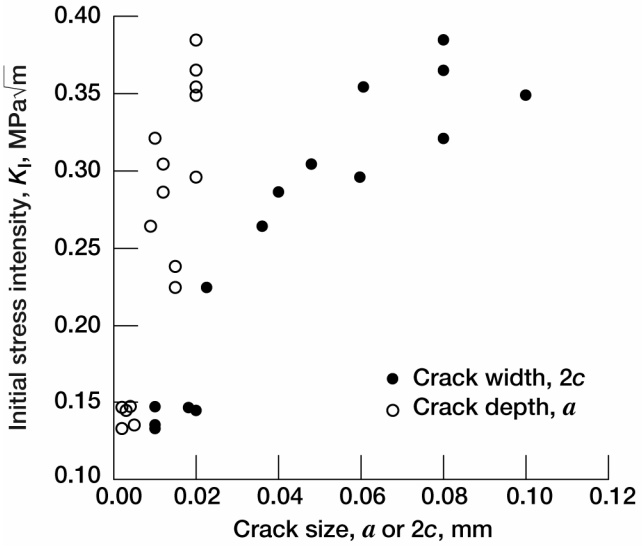

Figure 6.—Initial stress intensity K_I as function of initial crack size *a* or 2*c* for ZnSe in air based on constant-stress data in table I of reference 11. Maximum stress intensity occurred at crack depth *a* in all but three cases.

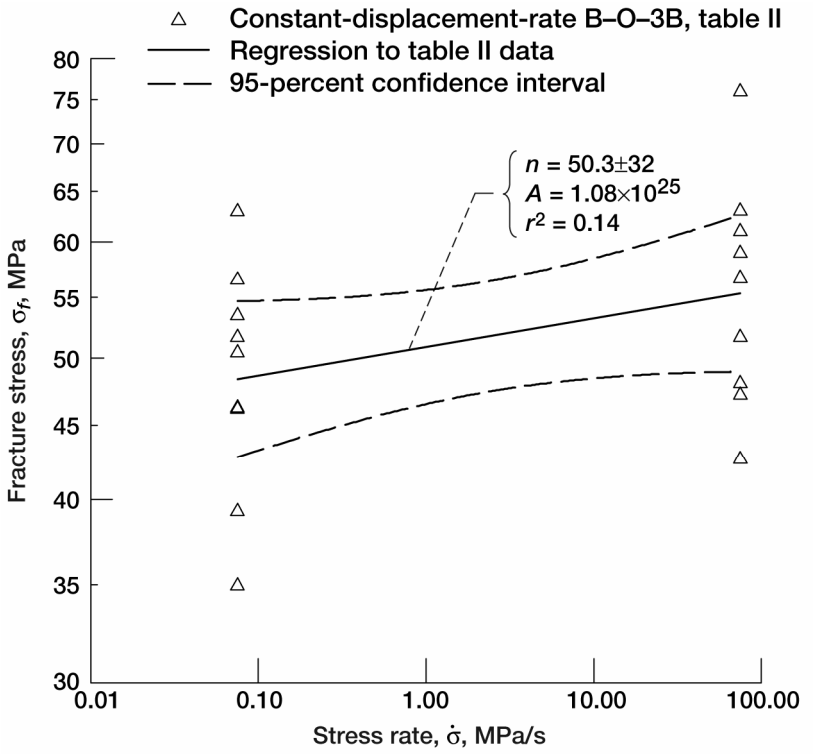

Figure 7.—Fracture stress σ_f as function of stress rate for ZnSe in water. Data is from table II. Single crystal fracture toughness of 0.33 MPa$\sqrt{m}$ was used to calculate parameter *A*. Regression curve was fit by least squares linear regression of equation (4). B–O–3B is point loading of circular plates supported by three balls.

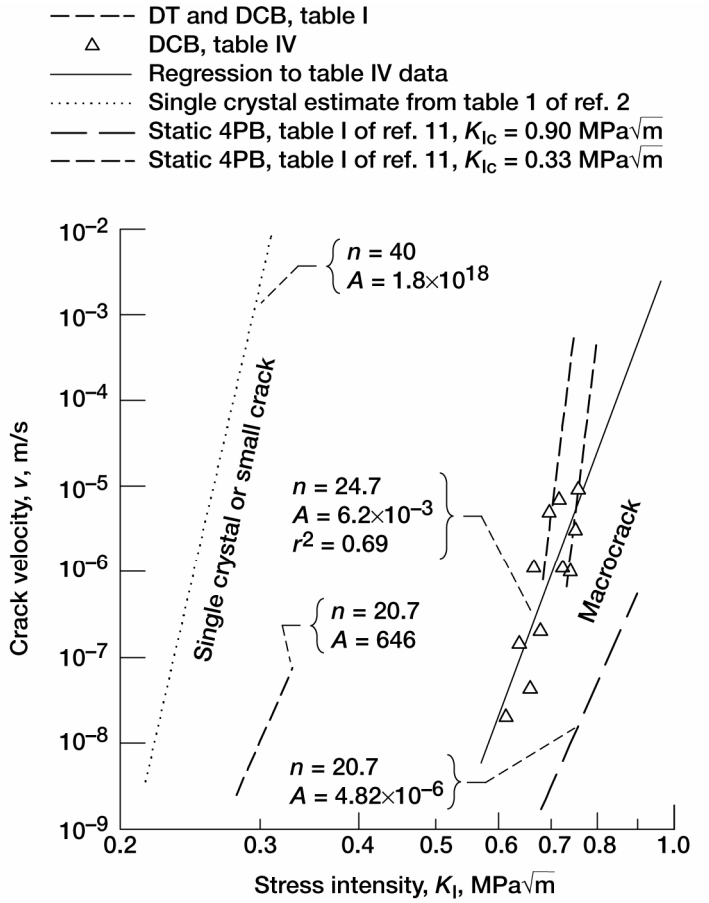

Figure 8.—Crack velocity v as function of stress intensity factor K_I for ZnSe in air from data in tables I and IV. Solid line is data from table IV fit by least squares linear regression of equation (2). Dotted line plots equation (1) with parameters from table 1 of reference 2. DCB is double-cantilever beam, and DT is double torsion. 4PB is four-point bending.

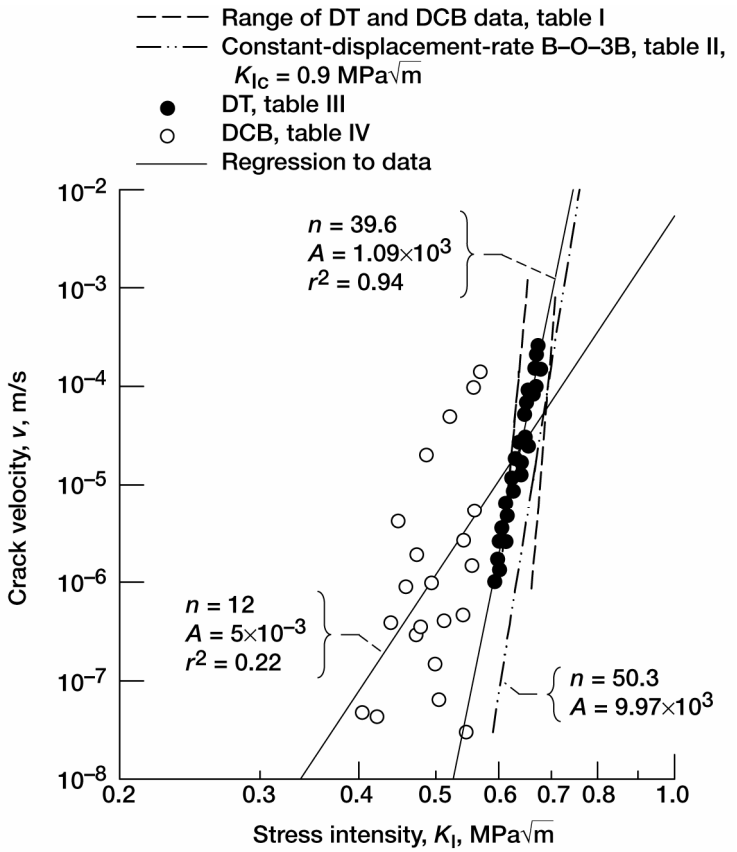

Figure 9.—Crack velocity v as function of stress intensity factor K_I for ZnSe in water for data in tables I to IV. Regression curves were fit by least squares linear regression of equation (2). DCB is double-cantilever beam, DT is double torsion, and B–O–3B is point loading of circular plates supported by three balls.

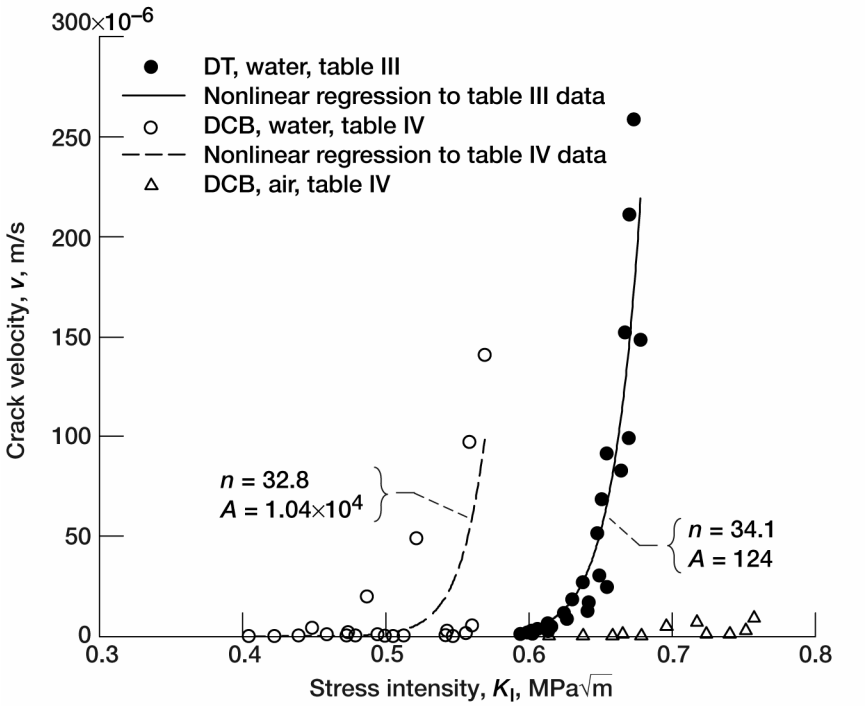

Figure 10.—Crack velocity v as function of stress intensity factor K_I for ZnSe in air and water for data in tables III and IV. DCB is double-cantilever beam, and DT is double torsion.

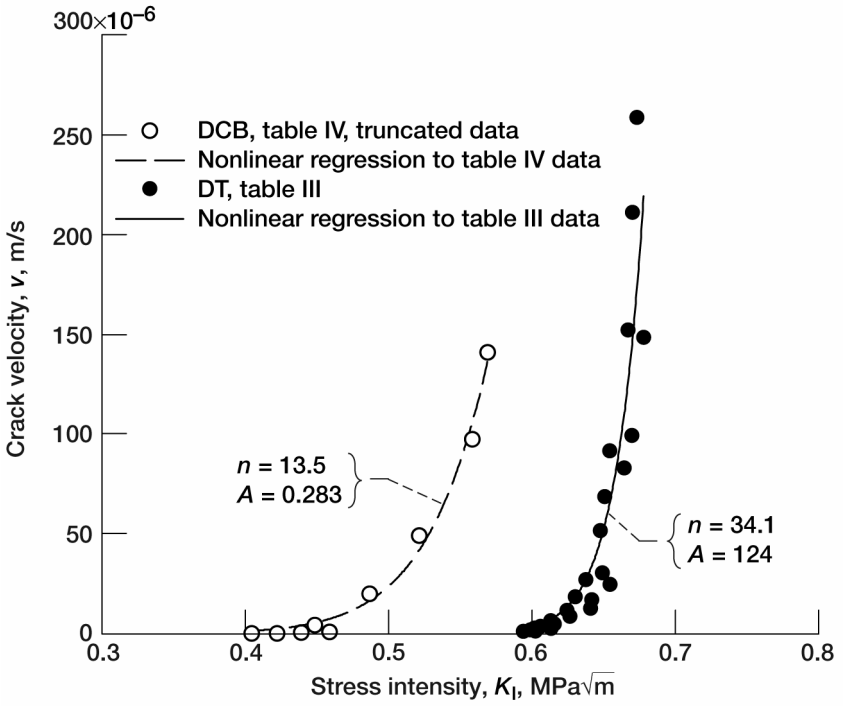

Figure 11.—Crack velocity v as function of stress intensity factor K_I for ZnSe in water for data in tables III and IV. Low-velocity, high-K_I data from reference 2 has been truncated. DCB is double-cantilever beam, and DT is double torsion.

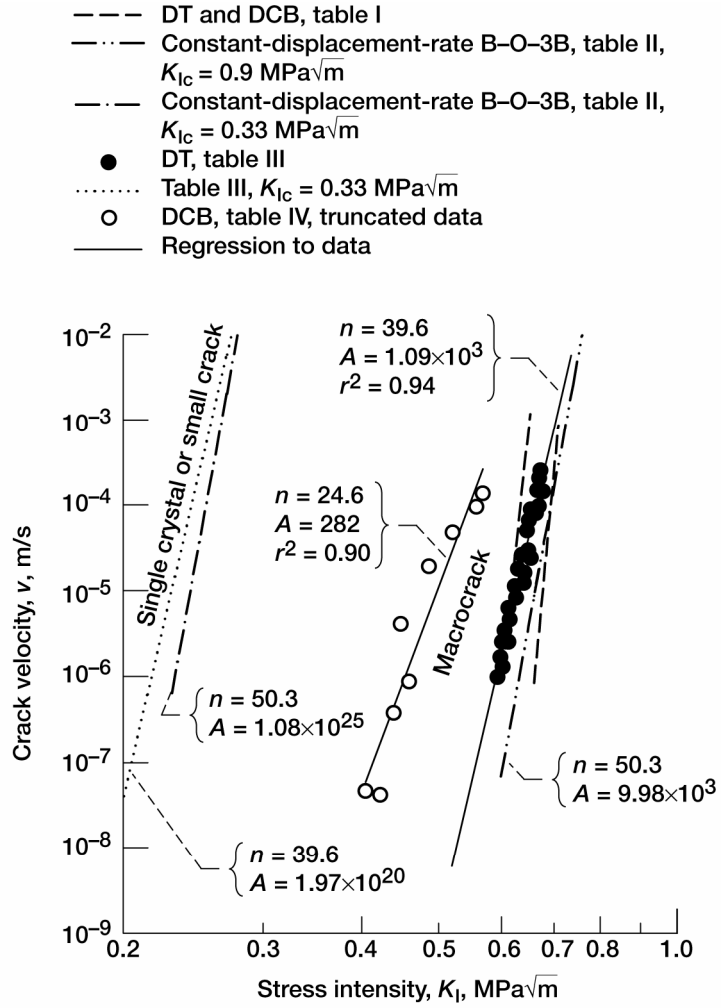

Figure 12.—Crack velocity v as function of stress intensity factor K_I for ZnSe in water for parameters in table XII. DCB is double-cantilever beam, DT is double torsion, and B–O–3B is point loading of circular plates supported by three balls. Data points shown are from tables III and IV. Low-velocity, high-K_I data from reference 2 has been truncated. Single crystal lines were estimated from constant-displacement-rate and DT data of reference 1 and the single crystal fracture toughness of reference 2.

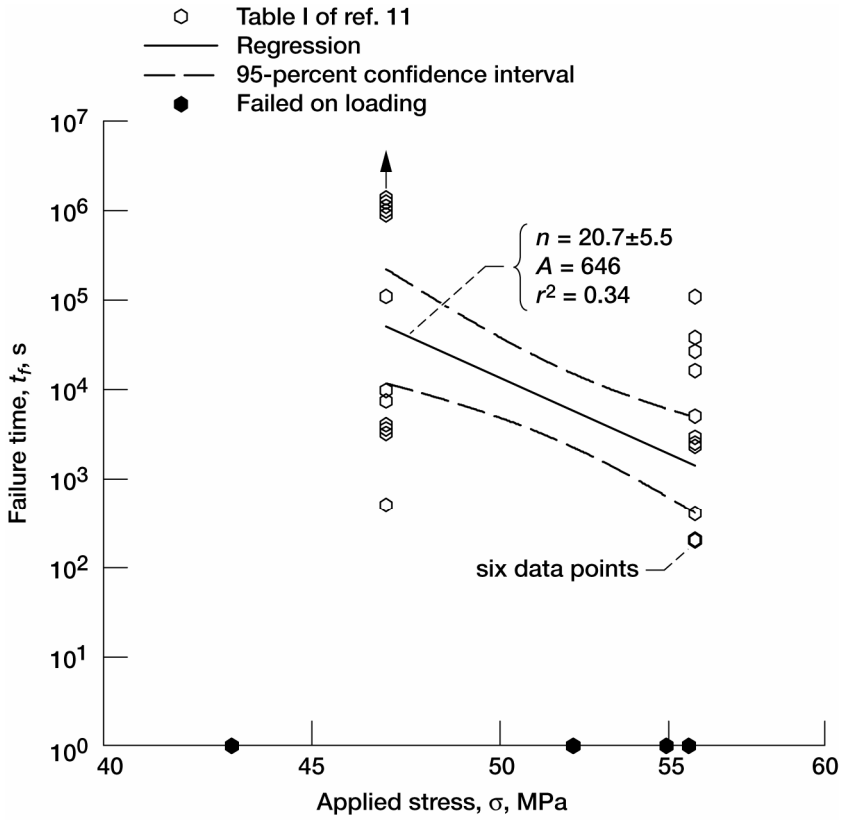

Figure 13.—Failure time t_f as function of static stress σ on ZnSe in air. Failure times of less than 200 s were not used in regression analysis because they did not represent long-term intergranular crack growth. Single crystal fracture toughness of 0.33 MPa$\sqrt{m}$ was used to calculate parameter A. Regression curve was fit by least squares linear regression of equation (7).

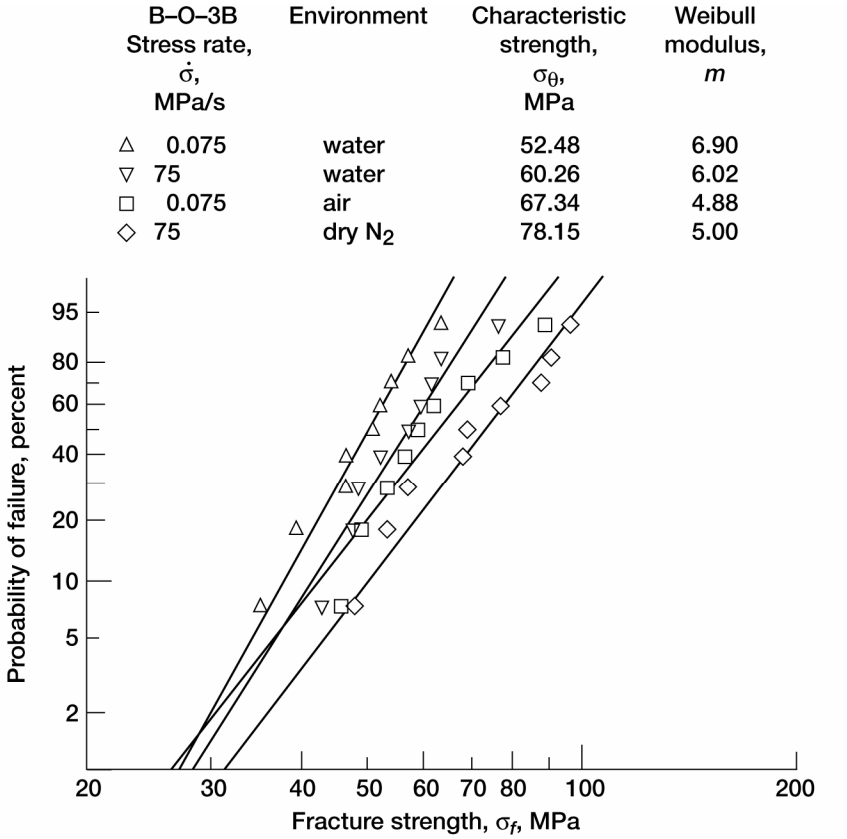

Figure 14.—Weibull plot of fracture strength data from table II as measured by constant-displacement-rate testing of polished ZnSe disks. Values in legend were generated via maximum likelihood estimator. B–O–3B is point loading of circular plates supported by three balls.

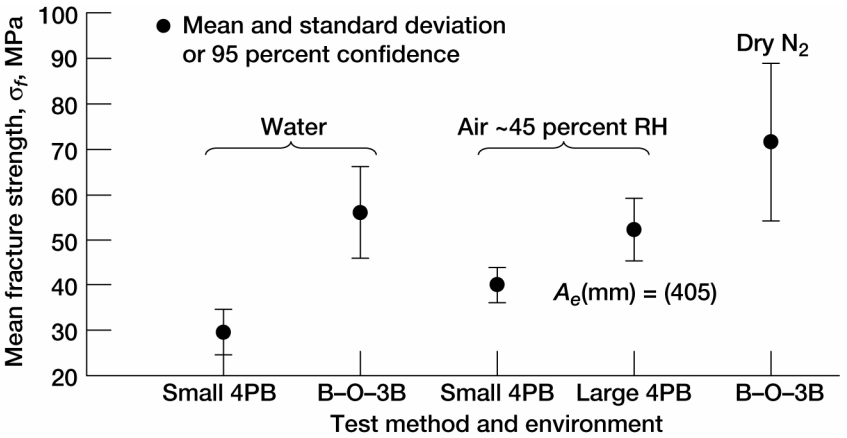

Figure 15.—Mean strength of CVD ZnSe as reported in references 1 to 3. 4PB is four-point bending, and B–O–3B is point loading of circular plates supported by three balls.

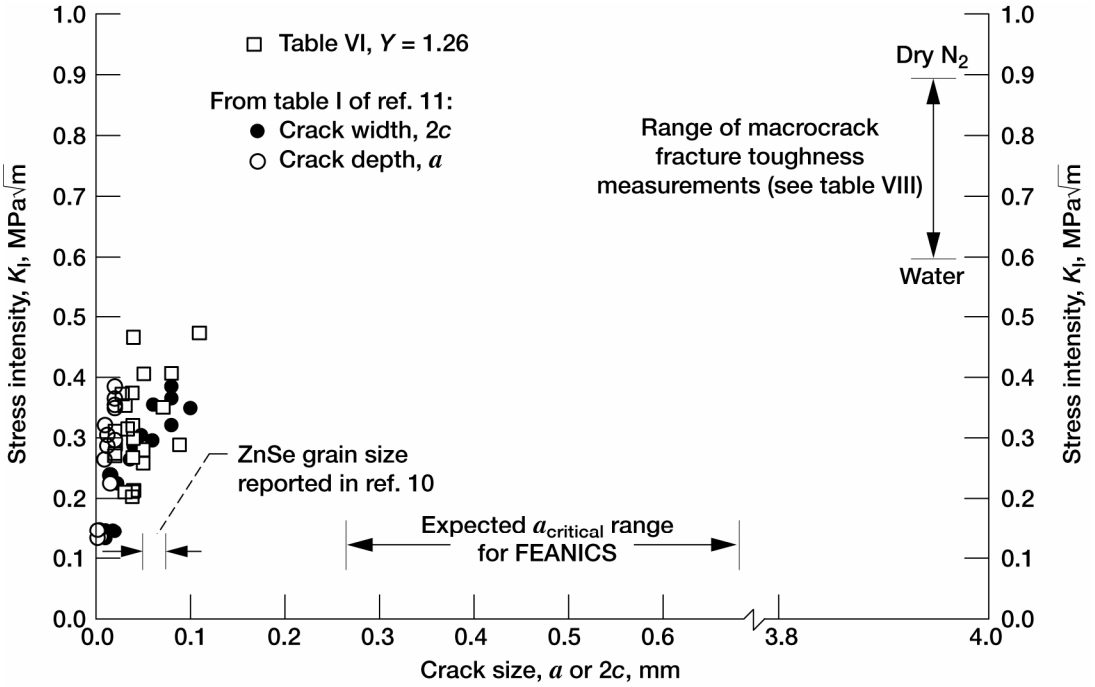

Figure 16.—Initial stress intensity K_I and fracture toughness K_{Ic} values of ZnSe as function of crack size a or $2c$ compared to expected critical flaw size $a_{critical}$ in FEANICS windows. A value of $Y = 1.26$ was used to estimate K_{Ic} values from table VI.

REPORT DOCUMENTATION PAGE

Form Approved
OMB No. 0704-0188

1. AGENCY USE ONLY (*Leave blank*)	2. REPORT DATE	3. REPORT TYPE AND DATES COVERED
	April 2005	Technical Memorandum

4. TITLE AND SUBTITLE

Estimation of ZnSe Slow-Crack-Growth Properties for Design of the Flow Enclosure Accommodating Novel Investigations in Combustion of Solids (FEANICS) Windows

5. FUNDING NUMBERS

WBS–22–400–35–40–07

6. AUTHOR(S)

Jonathan A. Salem

7. PERFORMING ORGANIZATION NAME(S) AND ADDRESS(ES)

National Aeronautics and Space Administration
John H. Glenn Research Center at Lewis Field
Cleveland, Ohio 44135–3191

8. PERFORMING ORGANIZATION REPORT NUMBER

E–14827

9. SPONSORING/MONITORING AGENCY NAME(S) AND ADDRESS(ES)

National Aeronautics and Space Administration
Washington, DC 20546–0001

10. SPONSORING/MONITORING AGENCY REPORT NUMBER

NASA TM—2005-213359

11. SUPPLEMENTARY NOTES

Responsible person, Jonathan A. Salem, organization code RSL, 216–433–3313.

12a. DISTRIBUTION/AVAILABILITY STATEMENT

Unclassified-Unlimited
Subject Category: 27

Available electronically at http://gltrs.grc.nasa.gov

This publication is available from the NASA Center for AeroSpace Information, 301–621–0390.

12b. DISTRIBUTION CODE

13. ABSTRACT ***(Maximum 200 words)***

This report reviews some of the literature on the fracture strength, fracture toughness, and crack growth properties of chemical-vapor-deposited ZnSe. The literature was reviewed to determine if the existing data on ZnSe is adequate to design windows for the Flow Enclosure Accommodating Novel Investigations in Combustion of Solids (FEANICS) project. Unfortunately, most of the published reports do not give all of the necessary design parameters despite having measured the data to do so. Further, the original data is not available. The data tabulated herein was determined by digitizing plots in original reprints of the publications. Based on the published data, an estimate of the slow-crack-growth parameters for small cracks in 100 percent humidity was made. For 100 percent humidity, the slow-crack-growth parameters n and A for small crack (or single crystal) failure were estimated. Weibull moduli estimated from bending of beams and circular plates ranged from 4 to 9, while fracture strengths ranged from 29 MPa in water to 72 MPa in dry nitrogen. Fracture toughness measurements yielded ranges, with the lower values representing failure from small flaws within grains and the larger values representing macroscopic cracks. Much of the data analyzed exhibited significant scatter, and the standard deviations were very large.

14. SUBJECT TERMS

Zinc selenide; Flexural strength; Fracture toughness; Crack propagation; Stress corrosion; Fatigue life; Weibull; Structural reliability

15. NUMBER OF PAGES

35

16. PRICE CODE

17. SECURITY CLASSIFICATION OF REPORT	18. SECURITY CLASSIFICATION OF THIS PAGE	19. SECURITY CLASSIFICATION OF ABSTRACT	20. LIMITATION OF ABSTRACT
Unclassified	Unclassified	Unclassified	